

RESEARCH ARTICLE

Anaerobiosis favors biosynthesis of single and multi-element nanostructures

Mirtha Ríos-Silva^{1,2}, Myriam Pérez¹, Roberto Luraschi¹, Esteban Vargas³, Claudia Silva-Andrade⁴, Jorge Valdés⁴, Juan Marcelo Sandoval⁵, Claudio Vásquez^{1†}, Felipe Arenas^{1*}

1 Laboratorio de Microbiología Molecular, Departamento de Biología, Facultad de Química y Biología, Universidad de Santiago de Chile, Santiago, Chile, **2** Research Center on the Intersection in Plasma Physics, Matter and Complexity, P²mc, Comisión Chilena de Energía Nuclear, Santiago, Chile, **3** Center for the Development of Nanoscience and Nanotechnology (CEDENNA), Santiago, Chile, **4** Centro de Genómica y Bioinformática, Universidad Mayor, Santiago, Chile, **5** Facultad de Ciencias, Universidad Arturo Prat, Iquique, Chile

† Deceased.

* felipe.arenas@usach.cl



OPEN ACCESS

Citation: Ríos-Silva M, Pérez M, Luraschi R, Vargas E, Silva-Andrade C, Valdés J, et al. (2022) Anaerobiosis favors biosynthesis of single and multi-element nanostructures. *PLoS ONE* 17(10): e0273392. <https://doi.org/10.1371/journal.pone.0273392>

Editor: Erika Kothe, Friedrich Schiller University, GERMANY

Received: June 9, 2021

Accepted: August 8, 2022

Published: October 7, 2022

Peer Review History: PLOS recognizes the benefits of transparency in the peer review process; therefore, we enable the publication of all of the content of peer review and author responses alongside final, published articles. The editorial history of this article is available here: <https://doi.org/10.1371/journal.pone.0273392>

Copyright: © 2022 Ríos-Silva et al. This is an open access article distributed under the terms of the [Creative Commons Attribution License](https://creativecommons.org/licenses/by/4.0/), which permits unrestricted use, distribution, and reproduction in any medium, provided the original author and source are credited.

Data Availability Statement: All relevant data are within the paper and its [Supporting Information](#) files. You can also go directly through the following link, in which all contigs are available with their

Abstract

Herein we report the use of an environmental multimetal(loid)-resistant strain, MF05, to biosynthesize single- or multi-element nanostructures under anaerobic conditions. Inorganic nanostructure synthesis typically requires methodologies and conditions that are harsh and environmentally hazardous. Thus, green/eco-friendly procedures are desirable, where the use of microorganisms and their extracts as bionanofactories is a reliable strategy. First, MF05 was entirely sequenced and identified as an *Escherichia coli*-related strain with some genetic differences from the traditional BW25113. Secondly, we compared the CdS nanostructure biosynthesis by whole-cell in a design defined minimal culture medium containing sulfite as the only sulfur source to obtain sulfide reduction from a low-cost chalcogen reactant. Under anaerobic conditions, this process was greatly favored, and irregular CdS (ex. 370 nm; em. 520–530 nm) was obtained. When other chalcogenites were tested (selenite and tellurite), only spherical Se⁰ and elongated Te⁰ nanostructures were observed by TEM and analyzed by SEM-EDX. In addition, enzymatic-mediated chalcogenite (sulfite, selenite, and tellurite) reduction was assessed by using MF05 crude extracts in anaerobiosis; similar results for nanostructures were obtained; however Se⁰ and Te⁰ formation were more regular in shape and cleaner (with less background). Finally, the *in vitro* nanostructure biosynthesis was assessed with salts of Ag, Au, Cd, and Li alone or in combination with chalcogenites. Several single or binary nanostructures were detected. Our results showed that MF05 is a versatile anaerobic bionanofactory for different types of inorganic NS. synthesis.

Introduction

Inorganic nanostructures (NS) have gained prominence in industries due to their adjustable physicochemical characteristics [1]. These materials can comprise metals or non-metals or

respective sequences: <https://www.ncbi.nlm.nih.gov/nuccore/1679187305>.

Funding: This work received financial support from FONDECYT (Fondo Nacional de Ciencia y Tecnología) Regular 1160051 (CV), National doctoral scholarship CONICYT (Comisión Nacional de Investigación Científica y Tecnológica) 21170508 (MR), support from USA1799 Vridei (Vicerrectoría de Investigación, Desarrollo e Innovación) 021943CV_GO Universidad de Santiago de Chile (MR, CV), Basal FB0807 CEDENNA (EV) and Centro de Genómica y Bioinformática, Universidad Mayor (JV) is also acknowledged.

Competing interests: The authors have declared that no competing interests exist.

take the form of an oxide, hydroxide, chalcogenide, or phosphate compound [2]. Currently, biosynthetic nanostructures biosynthesized by cells and bacteriophages cover at least 55 elements in the periodic table, which involves 146 single-element and multi-element NS [3].

When exposed to metal and non-metal ions, microorganisms transport these ions into cells through membrane carriers. Alkali and alkaline earth metal cations are used by cells to maintain intracellular homeostasis, serve as cofactors in enzymatic reactions, and survive. However, the presence (above trace level) of transition-metal ions such as Cu^{2+} and Ag^+ , as well as post-transition metal ions like Zn^{2+} , Cd^{2+} , and Hg^{2+} , are toxic. Thus, cells have developed strategies to remove these toxic ions either by ion export using efflux pumps or by other protective mechanisms, such as the reduction of inorganic ions to their elemental forms [4].

Surprisingly, certain microorganisms can grow in the presence of different metal(loid)s, leading to multi-metal(loid) resistance (MMR). This phenotype is interesting when microorganisms are considered as possible factories to produce inorganic nanomaterials. In this line, bacteria-producing metal nanomaterials with antimicrobial properties are a realistic biotechnological promise toward sustainability [5]. Bacteria reduce metal ions, chalcogens oxyanions, or other elements using NADH- or NADPH-dependent reductases, catalases, and terminal oxidases or by non-enzymatic routes such as thiol groups, and phosphates, among others [6–9].

Chalcogens are of special interest since sulfur, selenium, and tellurium can generate semiconductor compounds [10]. A common aspect of chalcogens is their ability to form oxyanions in oxidation states +4 and +6, known as chalcogenites and chalcogenates. Of the three chalcogenites, the most complex to approach -from the biological point of view- is tellurite. In contrast, sulfite and selenite are essential and have well-known biological functions [11]. Moreover, chalcogens can often be in their elemental/zero-state (0) or as chalcogenides (-2) associated with metals, which are of great technological interest, e.g., chalcogenide-based Quantum Dots (QDs). Most studies on chalcogenite bioreduction and NS formation, have been carried out via four electrons of selenite or tellurite to their elemental forms Se^0 and Te^0 , respectively [12–16]. Moreover, some bacteria contain enzymes that carry out physiological reductions of 6 electrons, such as nitrate reductase or sulfite reductase [17].

Regarding nanobiosynthesis, CdS QDs have been synthesized in *E. coli* by directly administering H_2S and CdCl_2 [18], or other species such as *Stenotrophomonas maltophilia* dealing with cysteine and $\text{Cd}(\text{CH}_3\text{COO})_2$ [19] or *Acidithiobacillus thiooxidans* ATCC 19703 using S_8 , CdCl_2 , and glutathione at pH 2.3 [20]. On the other hand, CdSe or CdTe QDs biosynthesis has also been reported [21–24]. However, precursors usually used i.e. H_2S or cysteine, aren't cost-effective for larger-scale processes. Moreover, the electrical, optical, and catalytic properties of inorganic NS are dependent on their elemental composition, crystallinity, size, and shape. It is, thus, important to be able to experiment with which types of inorganic NS can be biosynthesized in a specific biological model, so we can rationally prepare NS for a given application [3]. Besides, considering that toxicity mechanisms are normally associated with oxidative stress, an interesting approach for NS biosynthesis is anaerobiosis.

In this study, we evaluated the MF05 strain as a bionanofactory under anaerobiosis. MF05 has an MMR phenotype and was able to synthesize single- and multi-element nanostructures such as CdS, Se^0 and Te^0 Ag, Au, Cu, Li, Se, Te, and NS including CdS, Li-S, Ag-S, Au-Se, Cu-Te, Ag-Te, and Cd-Se. This was based on its ability to reduce chalcogenites without electron leakage (under the absence of molecular oxygen) and its resistance to toxic metal ions. In this line, the MF05 strain was previously studied in the presence of oxygen, with MICs for gold, copper, selenite, and tellurite, which were 0.25, 6.25, 500, and 1 mM, respectively. These values are significantly higher than those of *E. coli* BW25113, which are 0.16, 1, 125, and 0.004 mM for gold, copper, selenite, and tellurite, respectively. Therefore, MF05 had a resistant

phenotype and displayed the ability to synthesize metal NS of Ag and Au in the presence of molecular oxygen, but it was not able to reduce tellurite or selenite to their elemental forms [25]. We hypothesized that by using whole cells or parts of them in the form of crude extracts under anaerobic conditions, we would be able to avoid leakage of electrons that occurs naturally in the process of reducing O₂ as an electron acceptor, and thus generate a more reducing environment.

Materials and methods

Bacterial strains and culture conditions

MF05 was previously aerobically characterized by Figueroa et al. 2018 [25] and *E. coli* BW25113 was used as a wild-type control bacterium. Cells were grown routinely at 37°C in either LB, M9 minimum, or modified M9 minimum (M9*) medium containing 1 mM Na₂SO₃ and 1 mM MgCl₂ (instead of MgSO₄). Growth in liquid medium was generally started with a 1% dilution of overnight grown cultures. For experiments under anaerobic conditions, a Coy anaerobic chamber (Coy Laboratory Products, Inc. Grass Lake, MI, USA) with a 100% N₂ internal atmosphere was used.

Growth curves

Every 30 minutes, the anaerobic and aerobic growth curves were spectrophotometrically monitored in two TECAN M100 Pro multi-plate readers, one of which was located inside the anaerobic Coy chamber.

Biogenic H₂S determination

H₂S release was evaluated as described by Narayanaswamy and Sevilla [26]. Cultures of 3 ml inoculated at 1% were grown in M9 or M9* medium in the presence or absence of O₂. H₂S was measured on filter papers that had been immersed in 0.1 M Pb(CH₃COO)₂ for 1 h and then dried at 60°C. These were placed on the top of the tube of each culture and were sealed using Breatheasy® membranes to allow the gas passage without affecting the kind of respiration that was being evaluated. The formation of black precipitates in the filter paper corresponded to lead sulfide (PbS). Filters were scanned at high resolution and analyzed with the ImageJ software.

Preparation of cell extracts

Starting with a 1% inoculum, cultures of 500 ml were grown for 12 h in anaerobiosis. They were collected in 50 ml Falcon tubes, covered, and centrifuged at 9,000 x g for 10 min at 4°C. Cells were suspended in a 50 mM Tris-HCl buffer (pH 7.4), supplemented with 0.1 mM PMSF. Cells were sonicated on ice inside the Coy chamber with four pulses of 20 s. Centrifugation at 9,000 x g for 15 minutes at 4°C was used to remove cell debris. The supernatant, containing soluble proteins, was considered the crude extract.

Enzymatic activity measurements

The reducing activities for chalcogenites present in crude extracts were analyzed in anaerobiosis at pH 9.0 because there was less reduction of controls without extracts. The reactions were carried out in a final volume of 200 µL and monitored spectrophotometrically with a TECAN M100 Pro multi-plate reader based on the specific conditions for each chalcogenite:

For sulfite: 5 mM Na₂SO₃, 0.5 mM NAD(P)H, 0.5 mM β-mercaptoethanol (2-ME), and 25 μL of crude extract and buffer were used in the reaction. NAD(P)H consumption at 340 nm was measured every 30 s for 5 min.

For selenite: 1 mM Na₂SeO₃, 0.5 mM NAD(P)H, 0.5 mM 2-ME, and 25 μL of crude extract and buffer were used in the reaction. Measurements were made at 400 nm, whose peak represents elemental selenium formation (Se⁰), every 30 s for 5 min.

For tellurite: 1 mM Na₂TeO₃, 0.5 mM NAD(P)H, 0.5 mM 2-ME, and 25 μL of crude extract and buffer were used in the reaction. Measurements were made at 500 nm, whose peak represents elemental tellurium formation (Te⁰), every 30 s for 5 min.

An enzyme unit (U) was defined as the amount of enzyme needed to increase (and decrease in the case of sulfite) by 0.001 units of absorbance in 1 min.

NS synthesis and purification

Cell cultures NS synthesis. For NS synthesis and characterization, sulfite concentrations determined by the whole-cell system in a checkerboard format were considered for CdS formation, which corresponded to 864 μM CdCl₂ in the presence or absence of Na₂SO₃ up to 14.58 mM (sulfite incorporated into the medium). For both, selenite and tellurite, the concentration used was 1 mM. The concentrations used for lithium, gold, silver, and copper salts were 125 mM, 500 μM, 4 mM, and 4 mM, respectively.

Purification of whole-cell synthesized NS. Cultures of 200 mL were grown to a stationary phase to be treated with cadmium and chalcogenites. Cells were collected in 50 mL Falcon tubes at 9,000 x g for 10 minutes at 4°C, then suspended in 1 ml of 50 mM Tris-HCl buffer pH 7.4. Samples were sonicated on ice with 4 pulses of 1 min. In parallel, one day before the ultracentrifugation, a sucrose gradient was made with cushions of 20, 40, 50, and 60% in 5 ml tubes so that they were previously equilibrated overnight at 4°C. Samples of 800 μl were deposited on top of gradients and centrifuged at 300,000 x g for 2 h in a swinging-bucket rotor without brake. After centrifugation, tubes were observed with a UV transilluminator to detect those fractions displaying fluorescence. Around 25 fractions (200 μL each) were collected for future characterizations.

In vitro NS synthesis. From the enzymatic activity results, MF05 crude extracts were obtained to make checkerboards with NADH or NADPH for CdCl₂ with Na₂SO₃, Na₂SeO₃, or Na₂TeO₃, which were tested for 24 h at 37°C with constant agitation in anaerobiosis. For the assay, in a final volume of reaction of 200 μL, 0.5 mM NAD(P)H, 0.5 mM 2-ME and crude extracts (25 μl) were combined with CdCl₂: 0, 54, 108, 215, 432, or 864 μM; Na₂SO₃: 0, 0.5, 1 or 5 mM; and Na₂SeO₃ or Na₂TeO₃: 0, 0.5, 1 or 2 mM, and glycine buffer pH 9.0. After treatments, samples were visualized under visible or UV light. Then, excitation and emission fluorescence scan spectra were carried out to choose optimal concentrations of cadmium and/or chalcogenites and select them for electron microscopy characterization.

Fluorescence of biosynthesized QDs

Samples were observed in a UV transilluminator (λ_{exc} 254 nm) to determine the wavelength at which they emitted. Subsequently, an approximated emission wavelength was set to make an excitation scan. Finally, the wavelength of higher excitation was selected to scan the emission and determine precisely the emission wavelength. These determinations were carried out using the TECAN Infinite M200 Pro fluorimeter.

Transmission electron microscopy (TEM)

The NS generated from cell cultures were observed using a Hitachi HT7700 transmission electron microscope. Each sample was prepared by depositing ~20 μl of NS suspension in a copper

grid (200 mesh) using a continuous carbon film or lacey carbon. The analyses were carried out at the "Center for the Development of Nanoscience and Nanotechnology"—CEDENNA, USACH.

Determination of the chemical composition of NS by X-ray energy dispersion spectroscopy (EDX)

Approximately 20 μL of samples containing NS, as well as their respective controls, were deposited on a conductive carbon adhesive on a support pin. Scanning electron microscopy (SEM) analyses were performed using a Zeiss EVO MA-10 microscope with a tungsten filament gun and an energy dispersive X-ray (EDX) spectrum. Data was collected using an Oxford instrument X-ray system (connected to a microscope equipped with a Penta FET precision detector). Images were taken from the samples at an acceleration voltage of 20 kV and 8 mm working distance. Analyses were carried out at the "Center for the Development of Nanoscience and Nanotechnology", CEDENNA, USACH.

Sequencing, annotation, and comparative genomics

Genomic DNA from MF05 was extracted using Wizard[®] Genomic DNA Purification Kit (Promega). The QuantiFluor fluorometer was used to calculate concentration. Libraries were prepared with TruSeq Nano DNA Library Prep Kit (Illumina). For quality control of DNA libraries, size, distribution, and integrity of fragments were analyzed with 2100 Bioanalyzer Instrument (Agilent) with an average size of 407 bp. Sequencing was carried out using Illumina HiSeq. Contig assembly was compared by BlastX with the NR, Uniref100, and SwissProt databases. From the annotation, a comparison was made with *E. coli* K-12 BW25113 by Cluster of Orthologous Groups (COGs).

Data analysis

Plots and statistical analyses were carried out using GraphPad Prism 6.0 (GraphPad Software, Inc.) or Excel (Microsoft Office 365, Microsoft Corporation). Statistical analysis was used considering significance as follows: *, $p < 0.05$, **, $p < 0.01$, ***, $p < 0.001$ and ns, no significant difference.

Results

Identification of MF05 strain

MF05 is an environmentally isolated strain with an MMR phenotype. So firstly, the whole genome of MF05 was sequenced. Respective assemblies were carried out and it was found that it displayed size of 4,591,446 bp and 266 contigs, the longest being 414,005 base pairs. From this data, 4,389 genes were predicted, of which 4,312 hits against the nr database were detected when performing BlastP, and of these, 1,930 were hits for Proteobacteria, 1,608 for *E. coli*, and 522 for Enterobacteriaceae. Additionally, BlastX was performed against the nr and UniRef100 databases, in which 9,629 and 7,366 hits were displayed, respectively. When comparing the genome of MF05 with databases, the hits were mainly with *E. coli* and, to a lesser extent, with *Shigella* and Proteobacteria. Then, an ANI (Average Nucleotide Identity) analysis was performed among several strains such as *Acinetobacter schindleri*, *Salmonella bongori*, *S. enterica*, *Shigella sonnei*, *S. dysenteriae*, *S. flexneri*, six different strains of *E. coli*, and MF05. By previous bioinformatic analyses, a heatmap showed that MF05 showed identity with other strains of *E. coli* K-12 (Fig 1). Through ANI, it could be confirmed that the closest resemblance of MF05 is

	<i>Acinetobacter schindleri</i>	<i>Salmonella bongori</i>	<i>Salmonella enterica</i>	<i>Shigella dysenteriae</i>	<i>Shigella flexneri</i>	<i>Shigella sonnei</i>	<i>Escherichia coli</i> W3110	<i>Escherichia coli</i> MG1655	<i>Escherichia coli</i> BW25113	<i>Escherichia coli</i> BL21(DE3)	<i>Escherichia coli</i> O157:H7	<i>Escherichia coli</i> O104:H21	MF05
<i>Acinetobacter schindleri</i>	1.00000	0.71691	0.71289	0.71952	0.71960	0.70500	0.71518	0.71518	0.71518	0.71565	0.71713	0.71569	0.71363
<i>Salmonella bongori</i>	0.71691	1.00000	0.89541	0.80506	0.80440	0.78999	0.80428	0.80425	0.80425	0.80456	0.80332	0.80328	0.80403
<i>Salmonella enterica</i>	0.71356	0.89556	1.00000	0.81094	0.81033	0.78399	0.80934	0.80933	0.80929	0.81069	0.80878	0.80853	0.80872
<i>Shigella dysenteriae</i>	0.71761	0.80553	0.81377	1.00000	0.97597	0.96450	0.97959	0.97959	0.97966	0.97992	0.97826	0.97445	0.97960
<i>Shigella flexneri</i>	0.71324	0.80530	0.81268	0.97708	1.00000	0.96468	0.98259	0.98257	0.98259	0.98221	0.97825	0.98342	0.98259
<i>Shigella sonnei</i>	0.70500	0.79157	0.78560	0.96583	0.97385	1.00000	0.98067	0.98067	0.98067	0.97661	0.97591	0.97850	0.98067
<i>Escherichia coli</i> W3110	0.71645	0.80420	0.80898	0.97828	0.98121	0.97167	1.00000	0.99999	0.99999	0.99072	0.98093	0.98529	0.99987
<i>Escherichia coli</i> MG1655	0.71346	0.80434	0.80906	0.97851	0.98132	0.97158	1.00000	1.00000	0.99999	0.99106	0.98072	0.98539	0.99986
<i>Escherichia coli</i> BW25113	0.71669	0.80461	0.80872	0.97872	0.98118	0.97278	0.99999	0.99999	1.00000	0.99067	0.98092	0.98521	0.99982
<i>Escherichia coli</i> BL21(DE3)	0.71543	0.80483	0.81073	0.97852	0.98101	0.96356	0.99093	0.99093	0.99094	1.00000	0.98082	0.98499	0.99096
<i>Escherichia coli</i> O157:H7	0.71692	0.80216	0.80784	0.98024	0.97325	0.95946	0.97943	0.97944	0.97944	0.97697	1.00000	0.97485	0.97943
<i>Escherichia coli</i> O104:H21	0.71587	0.80362	0.80881	0.97677	0.98168	0.97145	0.98481	0.98481	0.98480	0.98432	0.97887	1.00000	0.98500
MF05	0.7003	0.8039	0.8090	0.9778	0.9810	0.9670	0.9997	0.9997	0.9997	0.9907	0.9805	0.9846	1.0000

Fig 1. Heatmap of ANI analysis for MF05 against 12 different proteobacteria strains. Nucleotide identity comparison between *Acinetobacter schindleri* ACE, *Salmonella bongori* NCTC 12419, *S. enterica* serovar Typhi CT18, *Shigella sonnei* BS1058, *S. dysenteriae* Sd197, *S. flexneri* 301, *E. coli* BW25113, *E. coli* MG1655, *E. coli* W3110, *E. coli* BL21 (DE3), *E. coli* O157:H7 Sakai, *E. coli* O104:H21 CSFSAN00236 and MF05.

<https://doi.org/10.1371/journal.pone.0273392.g001>

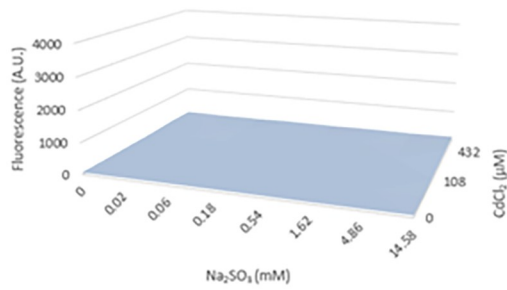
to *E. coli*. However, COG function analysis informed us that there are differences between MF05 and BW25113 (S1 Fig).

Whole-cell synthesis of chalcogen-based NS under anaerobiosis

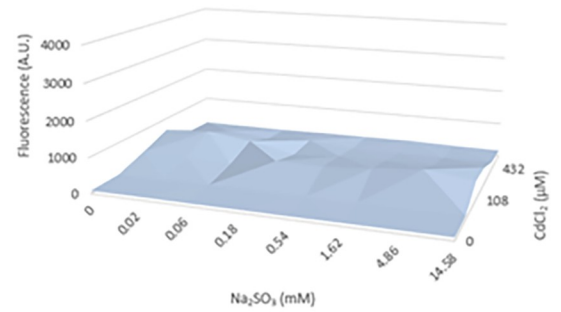
For nanostructure biosynthesis, the M9 medium avoids interferences during nucleation and growth processes. However, this medium contains magnesium sulfate, in which the sulfur oxidation state is +6. Therefore, M9 was modified, and magnesium sulfate was replaced by magnesium chloride and sodium sulfite, in which the sulfur oxidation state is +4 (hereafter M9*). Growth curves comparing M9 and M9* were assessed for MF05 and *E. coli* BW25113, both in aerobiosis and anaerobiosis, in which there was identical growth behavior in both media (S2 Fig). After that, checkerboards with increasing concentrations of sulfite and cadmium were carried out in M9 and M9* medium in aerobiosis and anaerobiosis. It was observed that in both media, *E. coli* BW25113 and MF05 did not show fluorescence when exposed to sulfite and cadmium in aerobiosis (Fig 2A, 2C, 2E and 2G). Conversely, anaerobic cultures in M9* medium showed significant fluorescence, both in *E. coli* BW25113 and MF05 (Fig 2F and 2H), indicating that this medium promotes the formation of CdS QDs, with CdCl₂ 864 μM and it does not require additional sulfite to that already contained in the medium.

To assess if M9* medium favors CdS QDs formation through a higher release of sulfide compounds, such as H₂S, a headspace detection test for MF05 was carried out with lead acetate using M9 or M9* media under aerobic and anaerobic conditions. In the absence of oxygen, greater PbS formation occurred when MF05 grew in M9*, which also happened, although to a lesser extent, in aerobiosis (Fig 3A). Thereafter, the time influence on fluorescence coming from CdS QDs formation was determined. To do so, the MF05 strain was grown in M9* to a stationary phase and treated with CdCl₂, as previously determined on checkerboards. Then, samples were collected several times post-treatment, and all samples displayed a similar fluorescence pattern, which decreased considerably at 24 h (Fig 3B). To determine at which wavelength CdCl₂-treated cultures were being excited and at which wavelength they emitted,

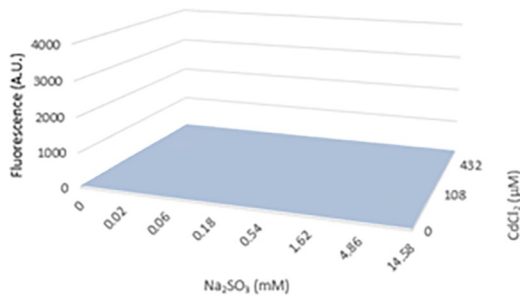
A *E. coli* BW25113/M9/+O₂



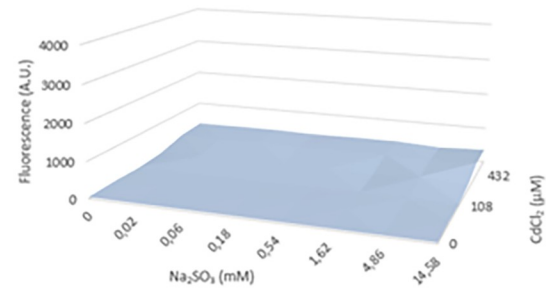
B *E. coli* BW25113/M9*/+O₂



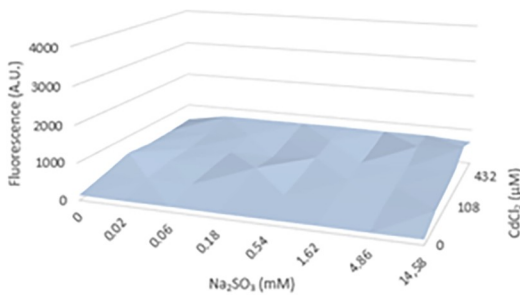
C MF05M9/+O₂/



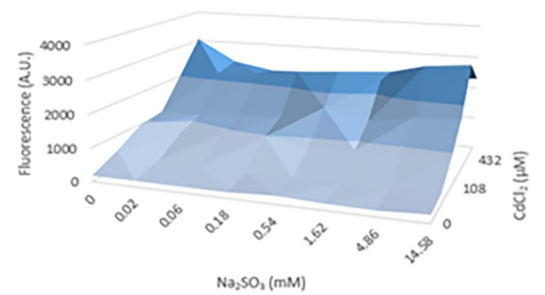
D MF05/M9*/+O₂



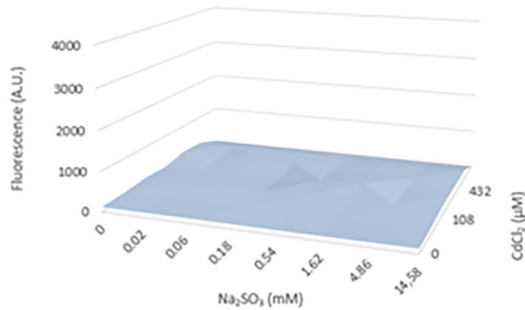
E *E. coli* BW25113/M9/-O₂



F *E. coli* BW25113/M9*/-O₂



G MF05/M9/-O₂



H MF05/M9*/-O₂

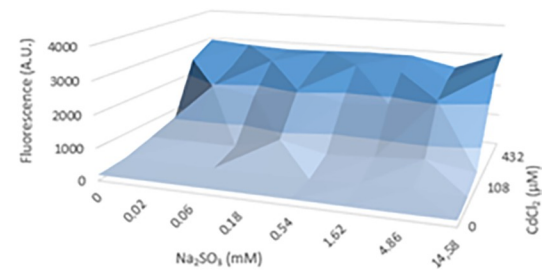


Fig 2. Fluorescence emission of sulfite and cadmium checkerboards to check CdS QDs formation by MF05 cells with M9 or M9* medium under aerobic or anaerobic conditions. Aerobic sulfite + CdCl₂ checkerboards assays for *E. coli* BW25113 grown in (A) M9 or (C) M9* medium, and MF05 grown in (E) M9 or (F) M9* medium. Anaerobic sulfite + CdCl₂ checkerboards assays for *E. coli* BW25113 in (B) M9 or (D) M9* medium, and MF05 grown in (F) M9 or (H) M9* medium. Fluorescence was monitored with 230 and 640 nm of excitation and emission wavelength, respectively. The results represent the average of 3 independent trials.

<https://doi.org/10.1371/journal.pone.0273392.g002>

excitation and emission scans of treated and untreated cells were performed. Cadmium-treated cells showed maximum excitation at 370 nm at all times tested. The highest peak observed was at 30 min, followed by 2 h (Fig 3C). Regarding emission, peak values ranged between 520 and 530 nm, except for 24 h samples, in which emission was lost (Fig 3D).

Once the time and compound concentrations were set, the CdS QDs biosynthesized samples were analyzed by electronic microscopes, TEM, and SEM. An abundant pattern of dense electron points was observed that represent irregular CdS QDs (Fig 4B), as compared with the untreated sample (Fig 4A). Regarding the chemical composition analysis as determined by EDX, in the untreated sample, the most prevalent element was carbon, followed by oxygen, sodium, chlorine, sulfur, phosphorus, and potassium. Meanwhile, treated samples showed all

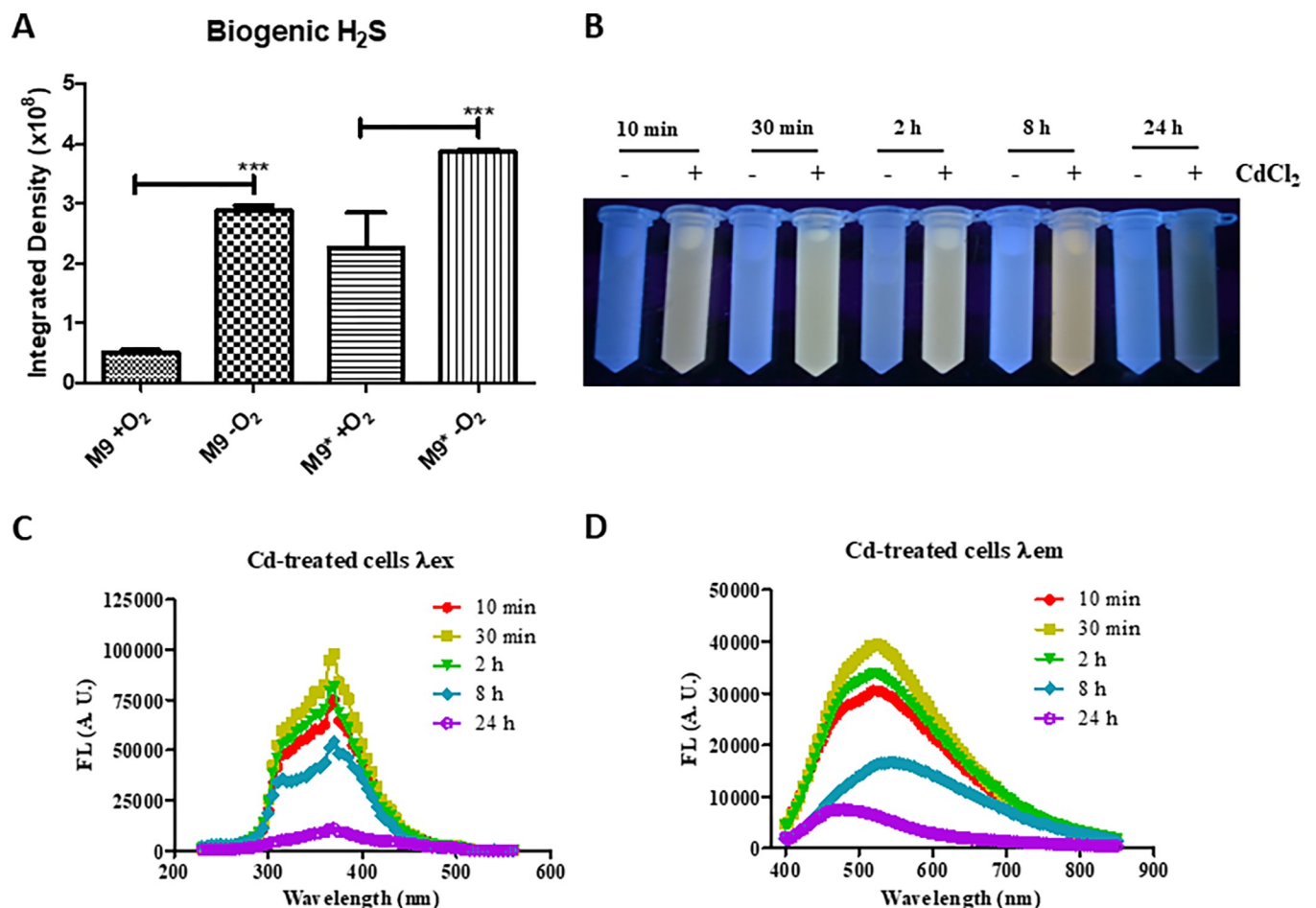


Fig 3. Release of H₂S by MF05 in M9 or M9* media, under aerobic or anaerobic conditions, and fluorescence tracing of CdS QDs formation at different times under anaerobic conditions. (A) Integrated density of image processing of H₂S release by MF05 cells grown in M9 or M9* medium under aerobic or anaerobic conditions with PbS filter papers. (B) CdS QDs formation after anaerobic growth of MF05 in M9* medium treated with 864 μM CdCl₂ with their respective negative controls. (C) Excitation and (D) emission spectra scan of Cd-treated MF05 cells. λ_{ex}: excitation with 590 nm emission wavelength; λ_{em}: emission with 370 nm excitation wavelength. For (A) the results represent the average of three independent trials ± SD ***, P < 0.001.

<https://doi.org/10.1371/journal.pone.0273392.g003>

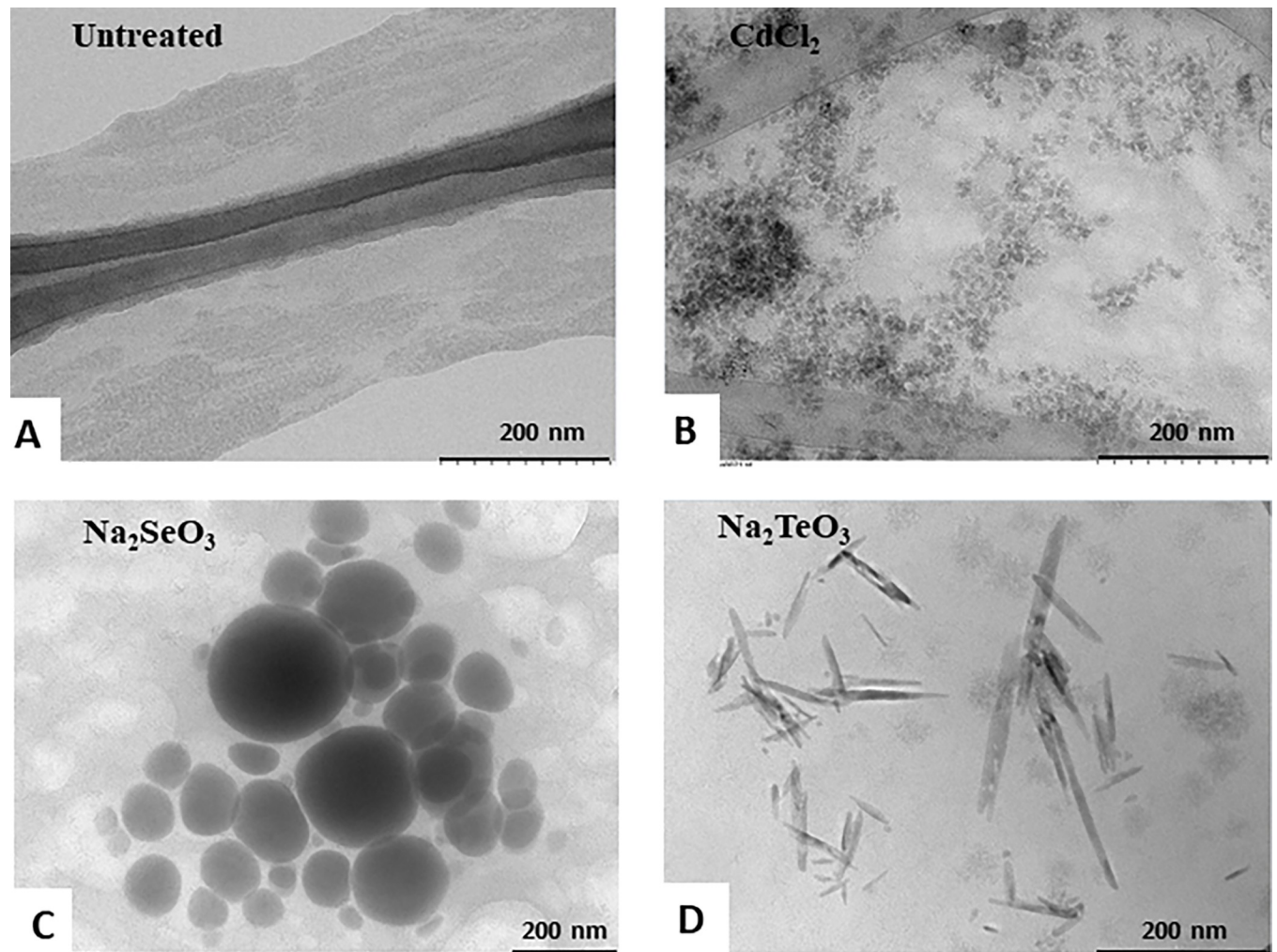


Fig 4. TEM NS of CdS QDs, Se, or Te by MF05 cells. Synthesis of NS by MF05 whole-cell in anaerobiosis (A) control and after treatments with (B) CdCl_2 ; (C) Na_2SeO_3 or (D) Na_2TeO_3 .

<https://doi.org/10.1371/journal.pone.0273392.g004>

the cellular elements and cadmium (S3 Fig). Given these results, we wanted to study the formation of other cadmium chalcogenides QDs (ex. CdSe and CdTe). However, in anaerobiosis, treatments with selenite or tellurite did not allow the clear formation of these QDs because the highest fluorescence exhibited at the lowest chalcogenite concentrations represented most probably CdS formation instead (S4 Fig). Despite being unable to synthesize whole-cell CdSe or CdTe QDs under these conditions, the formation of Se^0 and Te^0 NS by MF05 using M9* medium in anaerobiosis was carried out. It was observed that when exposed to selenite, electrodeposited elementary NS were formed with roughly spherical morphology (Fig 4C). In addition, tellurite treatment gave rise to an irregular, elongated NS (Fig 4D). In both cases, composition analysis showed the presence of chalcogens in addition to other organic elements (S3 Fig).

***In vitro* synthesis of metal or chalcogen-based NS by MF05**

As a cleaner alternative, *in vitro* synthesis was also considered. For these purposes, the reducing activities of chalcogenites of S, Se, and Te were examined. These assays were performed by

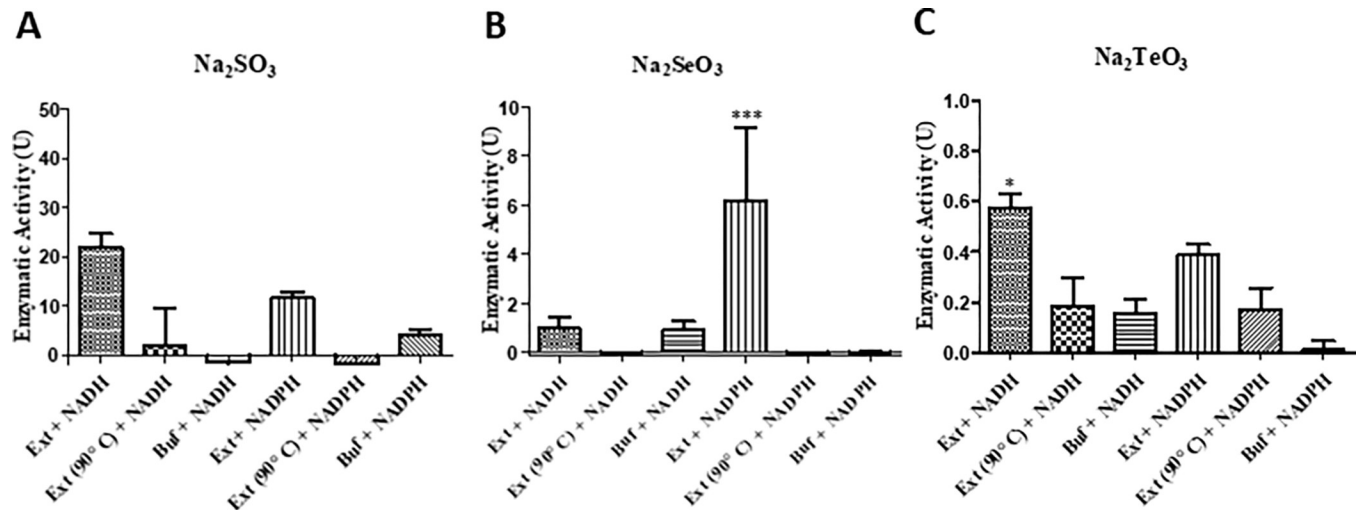


Fig 5. Chalcogenite-reducing activity assays in crude extracts of MF05 in anaerobiosis. Enzymatic activity by MF05 crude extracts for (A) sulfite reduction through NADH or NADPH consumption, (B) selenite reduction, through Se^0 formation, or (C) tellurite reduction through Te^0 formation. The results represent the average of three independent trials \pm SD. *, $P < 0.05$; *** $P < 0.001$.

<https://doi.org/10.1371/journal.pone.0273392.g005>

using crude extracts from MF05 cultures grown until the stationary phase in anaerobiosis. Controls contained only buffer or heated (90°C) crude extracts (as denatured proteins). The highest reducing activities for sulfite and tellurite were observed in the presence of NADH (Fig 5A and 5C), while for selenite, the best electron donor was NADPH (Fig 5B).

Then, cadmium-sulfite checkerboard assays were made using crude extracts with NADH or NADPH as electron donors. It was observed that when extracts were treated with NADH, 5 mM Na_2SO_3 , and CdCl_2 at 108, 216, 432, or 864 μM , there was fluorescence corresponding most probably to CdS QDs (S5 Fig). Complementing the above, samples were observed by TEM and analyzed by composition with SEM-EDX. No NS was observed in any of the controls (S6 Fig); NS formation upon co-treatment with cadmium and sulfite was evidenced (Fig 6A). To determine whether it was possible to synthesize CdSe or CdTe QDs *in vitro* using MF05 extracts, new checkerboard assays of $\text{Na}_2\text{SeO}_3 + \text{CdCl}_2$ or $\text{Na}_2\text{TeO}_3 + \text{CdCl}_2$ were constructed with NADH or NADPH. However, consistent with the previous results in whole-cell assays, treatment with selenite or tellurite allowed the formation of spherical NS corresponding to Se^0 or elongated NS corresponding to Te^0 (Fig 6B and 6C). In addition, anaerobic assays with additional metals were performed in which Ag^0 , Au^0 , and Cu^0 NS were produced (Fig 6D and 6F). It should be noted that results of biosynthesis from whole-cell, as determined by SEM-EDX for Se^0 and Te^0 , showed that their presence in the samples was 0.8% and 0.3%, respectively. In contrast, EDX results for Se^0 and Te^0 , for *in vitro* biosynthesis, exhibited values of 9.8% and 22.1%, respectively (S7 Fig). This comparison makes it possible to affirm that *in vitro* systems allow higher efficiency for synthesizing NS of zero-state chalcogens, in addition to lower complexity for purification.

Finally, an *in vitro* combination of metals and chalcogenites treatments was performed using crude extracts of MF05 in the anaerobiosis. Firstly, despite the high reactivity of lithium or lithium with sulfite, NS was formed (Fig 7A and 7B). Interestingly, the combination of silver + sulfite, gold + selenium, copper + tellurite, and silver + tellurite showed NS with similar patterns in which there are different areas of electron-density inside the same NS (Fig 7C–7F). These results suggest that the anaerobic conditions favor multi-element NS formation. Even though we could not detect fluorescence in samples exposed to cadmium + selenite or

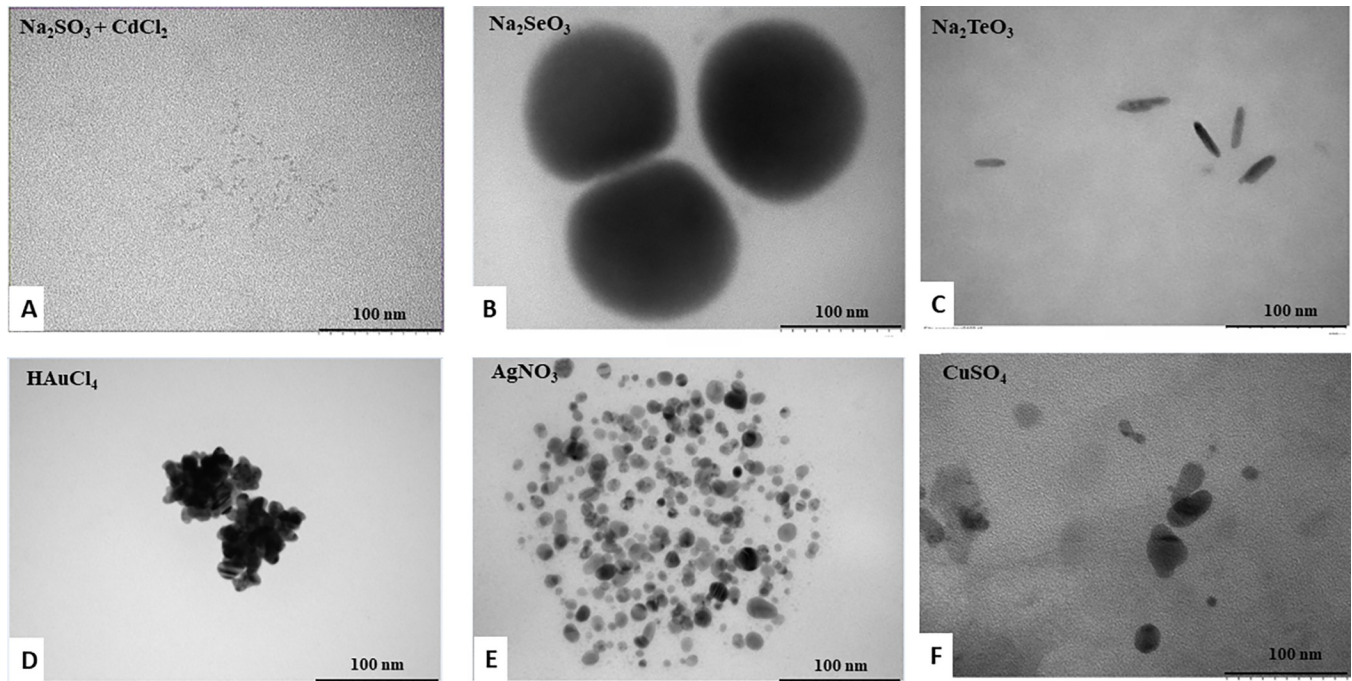


Fig 6. TEM of NS from *in vitro* synthesis by crude extracts of MF05. NS obtained after treatment with (A) $\text{Na}_2\text{SO}_3 + \text{CdCl}_2$; (B) Na_2SeO_3 ; (C) Na_2TeO_3 ; (D) HAuCl_4 ; (E) AgNO_3 or (F) CuSO_4 .

<https://doi.org/10.1371/journal.pone.0273392.g006>

cadmium + tellurite by whole-cells or *in vitro* synthesis. Thus, it is plausible that the alternative of bigger size NS in which the fluorescence properties of QDs can no longer be present. On one hand, treatment with selenite + cadmium showed very few single NS, which could be Se^0 or CdSe (Fig 7G). On the other hand, treatment with tellurite + cadmium evidenced two different shapes of NS; one was like that obtained before by whole-cell or *in vitro* synthesis with tellurite treatment, and the other with a spherical shape (Fig 7H). This result suggests that the absence of fluorescence in this sample was mainly due to Te^0 formation.

Discussion

As MMR microorganisms are an interesting target for NS synthesis as a response mechanism to the toxicity of different elements, this work studied reduction as a tool for the elaboration of inorganic (mainly chalcogen)-based nanomaterials such as QDs or elementary NS by the MF05 strain. The main disadvantage of using aerobic microorganisms is the toxicity of metal (loid)s, which is frequently associated with ROS formation [4]. One of the major challenges for chalcogenide-based NS generation is the reduction from chalcogenites (+4: SO_3^{2-} , SeO_3^{2-} , TeO_3^{2-}) to chalcogenides (-2: S^{2-} , Se^{2-} , Te^{2-}). Of the three chalcogens, tellurium is the most difficult to work with because it displays the lowest electronegativity and the highest toxicity to cells. As for tellurium and selenium, several studies have mainly focused on elemental (zero-state) NS formation under aerobic conditions [12, 14, 25]. Biologically, chalcogenite oxidation state has been observed in volatile compounds such as hydrogen sulfide, dimethyl sulfide, dimethylselenide, and dimethyltelluride [11, 27, 28]. Thus, QDs formation was considered as a six-electron reduction screening approach; from chalcogenite (+4) to chalcogenide (-2).

Since culture medium is essential for all bioprocesses, it should be noted that LB medium contains metals such as Mg, Ca, Fe, and Zn at micromolar levels and Co, Ni, Mn, Mo, and Cu

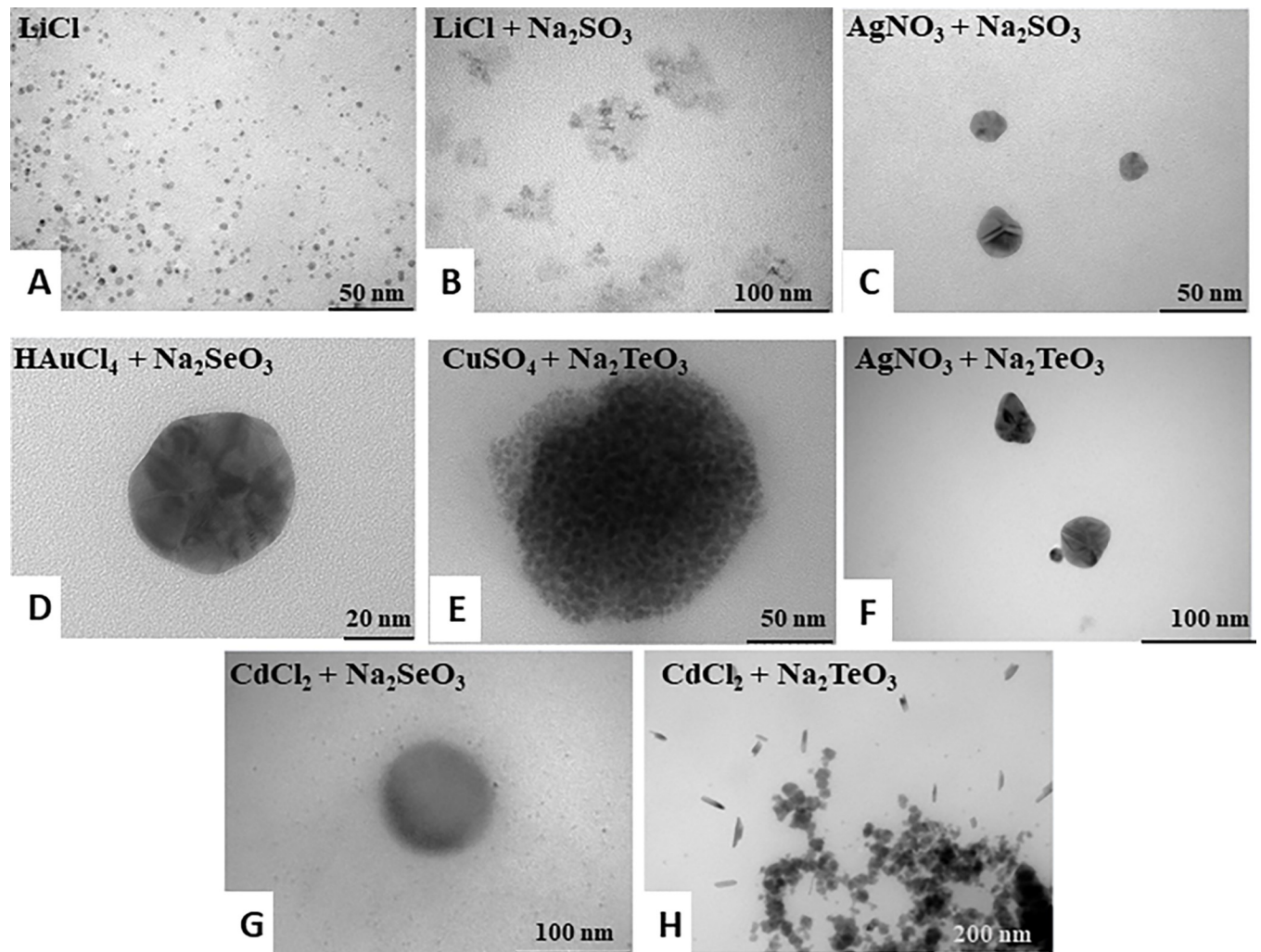


Fig 7. TEM of NS from *in vitro* synthesis by crude extracts of MF05. NS obtained after treatment with (A) LiCl; (B) LiCl + Na₂SO₃; (C) AgNO₃ + Na₂SO₃; (D) HAuCl₄ + Na₂SeO₃; (E) CdCl₂ + Na₂SeO₃; (F) CdCl₂ + Na₂TeO₃; (G) CuSO₄ + Na₂TeO₃; (H) AgNO₃ + Na₂TeO₃.

<https://doi.org/10.1371/journal.pone.0273392.g007>

at nanomolar levels, and it contains an estimated amount of cysteine of ~400 μM, which can be associated with copper, making it less available for cell entrance. This phenomenon could occur not only with copper but also with other divalent elements [29]. Due to the above, it was considered necessary to study bioreduction in a defined M9 minimal medium. Previous work showed that the high phosphate content of M9 medium favors the formation of cadmium phosphate by decreasing its solubility and rendering it less accessible to the cell. This more controlled entry of cadmium would favor subsequently formed CdS QDs [20]. Furthermore, previous investigations have used operationally expensive precursors or additional elements added to the medium, which decreases the cost-effective feasibility of NS synthesis [18–20]. Given that *E. coli* can synthesize CdS QDs under certain conditions [18], sulfite was used as a precursor because it is economical and is part of several metabolic pathways.

From group 16 of the Periodic Table, after oxygen, sulfur is the main chalcogen used by cells. For instance, sulfate assimilation mechanisms. However, there is another series of sulfur-based compounds known generically as reactive sulfur species (RSS), defined as "redox-active molecules that contain sulfur and that can, under physiological conditions, oxidize or reduce

biomolecules," including thiols, disulfides, sulfenic acid, thiosulfinate, thiosulfonate, thiyl radicals, and H₂S [30]. In this line, the biological system to obtain sulfides from sulfites or sulfates is further complicated. However, we can assert that more sulfides are being obtained given the presence of CdS QDs. Then, an interesting proposal would be to determine the efficiency within biological systems to analytically quantify the sulfite that is being reduced to sulfur, as well as what other sulfur-based precursors that are cost-effective could favor the observed phenotype.

In terms of bionanofactories, the cell itself generates confinement and energy change, which allows an open system with phase changes of solutions to precipitate that can allow the removal of products, such as NS, and thus favor their production. Regarding metal(loid)-chalcogenide synthesis, non-stoichiometric relationships favor the formation of more active axes within metal chalcogenide structures [31]. Chemical platforms, on the other hand, could not be extrapolated to a biological environment due to their high complexity and the multiple simultaneous processes that occur throughout the cell system. Besides, since sulfur is essential for life, it is not possible to remove it in cultures to test the other chalcogens. Therefore, it is likely that the product of chalcogen-based synthesis causes a mix between sulfur and selenium or tellurium. However, something remarkable in this whole-cell system was the stability of the particle size, since QDs kept their fluorescence properties for at least 10 weeks at 4 ° C. Fluorescence is directly related to particle size, so the bioprocess itself may confer biostabilizers to the particles, which could be very interesting to characterize.

Anaerobic reduction assays showed that sulfite reduction goes through enzymes that use NADH or NADPH as cofactors. Meanwhile, selenite reduction seems to prefer NADPH and tellurite reduction to NADH, suggesting that a common reduction mechanism is somehow unlikely. Experimentally, there were some drawbacks to the *in vitro* assays; for instance, sulfite can only be measured indirectly through oxidation of NADH or NADPH, while in the case of selenite and tellurite, the generation of their elemental forms can be determined spectrophotometrically. However, neither an increase of NAD(P)H oxidation nor the absence of Se⁰ or Te⁰ strongly suggests chalcogenide formation. In addition to chalcogenide detection mechanisms, it is interesting that the highest sulfite reduction was achieved using NADH since sulfite reductase uses NADPH as a cofactor.

Previous studies with MF05 showed that this strain does not exhibit remarkable reducing activities for selenite or tellurite aerobically, since these were not greater than 3 U/mg and 5 U/mg, respectively [25]. However, when performing the anaerobic tests with MF05, we could visualize elemental forms of both selenium and tellurium that are characteristic red-orange and black precipitates, respectively. Little information is available related to reducing activity in anaerobiosis, and it would be interesting to get proteomic data related to NS synthesis and metal exposure in anaerobic conditions. Furthermore, it would be interesting to identify which proteins are involved in the process, since heated cell extracts (with denatured proteins) showed lower activity in most cases.

From the results obtained by the genome analyses against several strains and more detailed against *E. coli* BW255113, it was possible to identify that the greatest difference between both strains lies in those genes that are not assigned a function by these databases, so it remains to identify which genomic elements could be granting the MMR phenotype and the ability to reduce chalcogenites and metals. Regarding cytotoxicity related to MF05, considering the possible uses in biomedicine, genome analyses showed that *stx1*, *stx2* or *eaeA* genes were not present in this strain (unpublished results). However, two different hemolysins (*hlyA*) were identified. Previous studies have concluded that *hly*-positive but *stx*-negative environmental isolates; also exhibit a certain degree of cytotoxicity [32], which should be considered if using a whole-cell system for NP synthesis. Moreover, the identification of new genetic determinants

that are associated with the synthesis of inorganic NS could be an interesting platform for new nanofabrication processes of structures of technological interest.

There is little information about the mechanisms of NS formation in biological systems; however, it is widely known that several reductases can reduce gold, copper, silver, and tellurium to their elemental forms [6–9, 33–36], which we were able to see as single NS for Se, Te, Li, Ag, Au, and Cu in MF05 under anaerobic conditions. Alternatively, a recent publication shows that the co-expression of metallothionein and phytochelatin synthase, in an aerobically grown recombinant *E. coli* strain, are involved in the biosynthesis of several single-element or multi-element NP, both in whole-cell and *in vitro* assays [37]. With the increased interest in NP production by biological process these structures had and will allow new industrial applications, such as antimicrobial (Ag-Au) and anticancer activities (Cu_2O), catalysis (dye degradation (Ag-Au-Pd), reduction of 4-nitrophenol (Au-Pd)), electrocatalysis (Au-Pd-Pt), chemiluminescence detection of glucose (Au-Ag) and adenine (Pt/X; X: Cu, Au, Ag), among others [38–42]. Thus, further studies must be conducted related to the compatibility of the biosynthesized nanostructures in our study for possible biomedical or industrial uses; however, several publications have proposed or demonstrated that CdS, Te, S, Au, Ag, and Cu NPs show application in diverse fields such as electronics and photonics (ex. solar cells and sensors), (bio)remediation of soil and water, agriculture, bioimaging, antimicrobial therapy and/or anti-cancer treatment [43–56].

Supporting information

S1 Fig. Clusters of Orthologous Groups (COGs). COG functions comparison for *E. coli* BW25113 (blue) and MF05 (orange).
(TIF)

S2 Fig. Growth curves of *E. coli* BW25113 and MF05 in M9 or M9* media. (A) Aerobic, (B) anaerobic *E. coli* BW25113, and (C) Aerobic, (D) MF05 cells grown in M9 (black circle) or M9* (inverted green triangle) medium. Each point represents the average of three independent trials \pm SD.
(TIF)

S3 Fig. SEM EDX of MF05 whole-cell samples after under anaerobic conditions treatment. Whole cells were (A) left untreated, exposed to (B) only CdCl_2 , (C) only Na_2SeO_3 or (D) only Na_2TeO_3 .
(TIF)

S4 Fig. Checkerboards fluorescence emission of Na_2SeO_3 and CdCl_2 or K_2TeO_3 and CdCl_2 under aerobic or anaerobic conditions for MF05 in M9* medium. Fluorescence was monitored with 230 and 640 nm of excitation and emission wavelength, respectively. Na_2SeO_3 + CdCl_2 in (A) aerobiosis or (B) anaerobiosis, and K_2TeO_3 + CdCl_2 in (C) aerobiosis and (D) anaerobiosis. The results represent the average of three independent trials.
(TIF)

S5 Fig. Excitation and emission fluorescence scan of sulfite and cadmium checkerboards for *in vitro* synthesis of CdS QDs with NADH or NADPH by crude extracts of MF05 under anaerobic conditions. Excitation (A and C) and emission (B and D) scan spectra of crude extracts of MF05 treated with Na_2SO_3 (S) and/or CdCl_2 (Cd) in the presence of NADH (A and B) or NADPH (C and D).
(TIF)

S6 Fig. TEM and SEM EDX of controls whole-cell assays in MF05. Whole cells were (A) left untreated, or exposed to (B) only CdCl₂ or (C) only Na₂SO₃. TEM (upper images) and SEM EDX (lower images) showed no formation of NP under these conditions. (TIF)

S7 Fig. SEM EDX of MF05 cell extract samples treatments under anaerobic conditions. Cells extracts were treated with (A) Na₂SO₃ + CdCl₂, (B) Na₂SeO₃, (C) Na₂TeO₃, (D) HAuCl₄, (E) AgNO₃ or (F) CuSO₄. (TIF)

Acknowledgments

Dr. Vásquez passed away before the submission of the final version of this manuscript. Dr. Arenas accepts responsibility for the integrity and validity of the data collected and analyzed.

We would also like to thank Fabián Araneda from CEDENNA for his assistance with the electron microscope operation and Dr. Natalia Valdés from Universidad de Santiago de Chile, Facultad de Química y Biología for her assistance with bioinformatics analyses.

This paper is dedicated to our beloved professor, Dr. Claudio Vásquez (R.I.P.)†. He firmly taught us science and life values.

Author Contributions

Conceptualization: Mirtha Ríos-Silva, Myriam Pérez, Claudia Silva-Andrade, Juan Marcelo Sandoval, Claudio Vásquez, Felipe Arenas.

Data curation: Mirtha Ríos-Silva, Myriam Pérez, Roberto Luraschi, Claudia Silva-Andrade, Felipe Arenas.

Formal analysis: Mirtha Ríos-Silva, Jorge Valdés, Juan Marcelo Sandoval, Felipe Arenas.

Funding acquisition: Esteban Vargas, Jorge Valdés, Claudio Vásquez, Felipe Arenas.

Investigation: Mirtha Ríos-Silva, Myriam Pérez, Roberto Luraschi, Esteban Vargas, Claudio Vásquez, Felipe Arenas.

Methodology: Mirtha Ríos-Silva, Myriam Pérez, Roberto Luraschi, Esteban Vargas, Claudia Silva-Andrade, Jorge Valdés, Claudio Vásquez, Felipe Arenas.

Project administration: Claudio Vásquez, Felipe Arenas.

Resources: Jorge Valdés, Claudio Vásquez, Felipe Arenas.

Software: Claudia Silva-Andrade.

Supervision: Juan Marcelo Sandoval, Felipe Arenas.

Validation: Esteban Vargas, Juan Marcelo Sandoval, Claudio Vásquez, Felipe Arenas.

Visualization: Esteban Vargas.

Writing – original draft: Mirtha Ríos-Silva, Claudio Vásquez, Felipe Arenas.

Writing – review & editing: Mirtha Ríos-Silva, Juan Marcelo Sandoval, Claudio Vásquez, Felipe Arenas.

References

1. Cao H. Synthesis and applications of inorganic nanostructures. JWS. 2017. ISBN: 978-3-527-69817-2.

2. Davies DW, Butler KT, Jackson AJ, Morris A, Frost JM, Skelton, et al. Computational screening of all stoichiometric inorganic materials. *Chem*. 2016; 1(4): 617–627. <https://doi.org/10.1016/j.chempr.2016.09.010> PMID: 27790643
3. Choi Y, Lee SY. Biosynthesis of inorganic nanomaterials using microbial cells and bacteriophages. *Nat Rev Chem*. 2020; 1–19.
4. Lemire JA, Harrison JJ, Turner RJ. Antimicrobial activity of metals: mechanisms, molecular targets and applications. *Nat Rev Microbiol*. 2013; 11(6): 371–384. <https://doi.org/10.1038/nrmicro3028> PMID: 23669886
5. Turner RJ. Metal-based antimicrobial strategies. *Microb Biotechnol*. 2017; 10(5): 1062–1065. <https://doi.org/10.1111/1751-7915.12785> PMID: 28745454
6. Turner RJ, Weiner JH, and Taylor DE. Selenium metabolism in *Escherichia coli*. *Biometals*. 1998; 11(3): 223–227.
7. Presentato A, Piacenza E, Turner RJ, Zannoni D, Cappelletti M. Processing of metals and metalloids by actinobacteria: cell resistance mechanisms and synthesis of metal (loid)-based nanostructures. *Microorganisms*. 2020; 8(12): 2027. <https://doi.org/10.3390/microorganisms8122027> PMID: 33352958
8. Durán N, Marcato PD, Durán M, Yadav A, Gade A and Rai M. Mechanistic aspects in the biogenic synthesis of extracellular metal nanoparticles by peptides, bacteria, fungi, and plants. *Appl Microbiol Biot*. 2011; 90(5): 1609–1624.
9. Pantidos N, Horsfall LE. Biological synthesis of metallic nanoparticles by bacteria, fungi and plants. *J Nanomed Nanotechnol*. 2014; 5(5): 10.
10. Murray C, Norris DJ and Bawendi MG. Synthesis and characterization of nearly monodisperse CdE (E = sulfur, selenium, tellurium) semiconductor nanocrystallites. *J Am Chem Soc*. 1993; 115(19): 8706–8715.
11. Chasteen TG, Fuentes DE, Tantaleán JC, Vásquez CC. Tellurite: history, oxidative stress, and molecular mechanisms of resistance. *FEMS Microbiol Rev*. 2009; 33(4): 820–832. <https://doi.org/10.1111/j.1574-6976.2009.00177.x> PMID: 19368559
12. Pugin B, Cornejo FA, Muñoz-Díaz P, Muñoz-Villagrán CM, Vargas-Pérez JI, Arenas FA, et al. Glutathione reductase-mediated synthesis of tellurium-containing nanostructures exhibiting antibacterial properties. *Appl Environ Microbiol*. 2014; 80(22): 7061–7070. <https://doi.org/10.1128/AEM.02207-14> PMID: 25193000
13. Mirjani R, Faramarzi MA, Sharifzadeh M, Setayesh N, Khoshayand MR and Shahverdi AR. Biosynthesis of tellurium nanoparticles by *Lactobacillus plantarum* and the effect of nanoparticle-enriched probiotics on the lipid profiles of mice. *IET Nanobiotechnol*. 2015; 9(5): 300–305.
14. Shirsat S, Kadam A, Naushad M, Mane RS. Selenium nanostructures: microbial synthesis and applications. *RSC Adv*. 2015; 5(112): 92799–92811.
15. Song D, Li X, Cheng Y, Xiao X, Lu Z, Wang Y, et al. Aerobic biogenesis of selenium nanoparticles by *Enterobacter cloacae* Z0206 as a consequence of fumarate reductase mediated selenite reduction. *Sci Rep*. 2017; 7(1): 1–10.
16. Wang X, Zhang D, Pan X, Lee DJ, Al-Misned FA, Mortuza MG, et al. Aerobic and anaerobic biosynthesis of nano-selenium for remediation of mercury contaminated soil. *Chemosphere*. 2017; 170: 266–273. <https://doi.org/10.1016/j.chemosphere.2016.12.020> PMID: 28011305
17. Crane BR, Getzoff ED. The relationship between structure and function for the sulfite reductases. *Curr Opin Struct Biol*. 1996; 6(6): 744–756. [https://doi.org/10.1016/s0959-440x\(96\)80003-0](https://doi.org/10.1016/s0959-440x(96)80003-0) PMID: 8994874
18. Sweeney RY, Mao C, Gao X, Burt JL, Belcher AM, Georgiou G, et al. Bacterial biosynthesis of cadmium sulfide nanocrystals. *Cell Chem Biol*. 2004; 11(11): 1553–1559. <https://doi.org/10.1016/j.chembiol.2004.08.022> PMID: 15556006
19. Yang Z, Lu L, Berard VF, He Q, Kiely CJ, Berger BW, et al. Biomanufacturing of CdS quantum dots. *Green Chem*. 2015; 17(7): 3775–3782.
20. Ulloa G, Quezada CP, Araneda M, Escobar B, Fuentes E, Álvarez SA, et al. Phosphate favors the biosynthesis of CdS quantum dots in *Acidithiobacillus thiooxidans* ATCC 19703 by improving metal uptake and tolerance. *Front Microbiol*. 2018; 9: 234.
21. Kumar SA, Ansary AA, Ahmad A, Khan MI. Extracellular biosynthesis of CdSe quantum dots by the fungus, *Fusarium oxysporum*. *J Biomed Nanotechnol*. 2007; 3(2): 190–194.
22. Monrás JP, Díaz V, Bravo D, Montes RA, Chasteen TG, Osorio-Román IO, et al. Enhanced glutathione content allows the in vivo synthesis of fluorescent CdTe nanoparticles by *Escherichia coli*. *PLoS One*. 2012; 7(11): e48657.
23. Pérez-Donoso JM, Monrás JP, Bravo D, Aguirre A, Quest AF, Osorio-Román IO, et al. Biomimetic, mild chemical synthesis of CdTe-GSH quantum dots with improved biocompatibility. *PLoS One*. 2012; 7(1): e30741. <https://doi.org/10.1371/journal.pone.0030741> PMID: 22292028

24. Yan ZY, Ai XX, Su YL, Liu XY, Shan XH, Wu SM. Intracellular biosynthesis of fluorescent CdSe quantum dots in *Bacillus subtilis*: a strategy to construct signaling bacterial probes for visually detecting interaction between *Bacillus subtilis* and *Staphylococcus aureus*. *Microsc Microanal Microstruct*. 2016; 22(1): 13–21.
25. Figueroa M, Fernandez V, Arenas-Salinas M, Ahumada D, Muñoz-Villagrán C, Cornejo F, et al. Synthesis and antibacterial activity of metal (loid) nanostructures by environmental multi-metal (loid) resistant bacteria and metal (loid)-reducing flavoproteins. *Front Microbiol*. 2018; 9: 959. <https://doi.org/10.3389/fmicb.2018.00959> PMID: 29869640
26. Narayanaswamy R and Sevilla F. Optosensing of hydrogen sulphide through paper impregnated with lead acetate. *Fresenius Z Anal Chem*. 1988; 329(7): 789–792.
27. Ranjard L, Prigent-Combaret C, Nazaret S, Cournoyer B. Methylation of inorganic and organic selenium by the bacterial thiopurine methyltransferase. *J Bacteriol*. 2002; 184(11): 3146–3149. <https://doi.org/10.1128/JB.184.11.3146-3149.2002> PMID: 12003960
28. Audrain B, Létoffé S, Ghigo JM. Airborne bacterial interactions: functions out of thin air? *Front Microbiol*. 2015; 6: 1476. <https://doi.org/10.3389/fmicb.2015.01476> PMID: 26733998
29. Nies DH, Herzberg M. A fresh view of the cell biology of copper in enterobacteria. *Mol Microbiol*. 2013; 87(3): 447–454. <https://doi.org/10.1111/mmi.12123> PMID: 23217080
30. Gruhke MC, Slusarenko AJ. The biology of reactive sulfur species (RSS). *Plant Physiol Bioch*. 2012; 59: 98–107. <https://doi.org/10.1016/j.plaphy.2012.03.016> PMID: 22541352
31. McAllister J, Bandeira NA, McGlynn JC, Ganin AY, Song YF, Bo C, et al. Tuning and mechanistic insights of metal chalcogenide molecular catalysts for the hydrogen-evolution reaction. *Nat Commun*. 2019; 10(1): 370. <https://doi.org/10.1038/s41467-018-08208-4> PMID: 30670694
32. Maldonado Y, Fiser JC, Nakatsu CH and Bhunia AK. Cytotoxicity potential and genotypic characterization of *Escherichia coli* isolates from environmental and food sources. *Appl Environ Microbiol*. 2005; 71(4): 1890–1898.
33. Ovais M, Khalil AT, Ayaz M, Ahmad I, Nethi SK, Mukherjee S. Biosynthesis of metal nanoparticles via microbial enzymes: a mechanistic approach. *Int J Mol Sci*. 2018; 19(12): 4100. <https://doi.org/10.3390/ijms19124100> PMID: 30567324
34. Koul B, Poonia AK, Yadav D, Jin JO. Microbe-Mediated Biosynthesis of Nanoparticles: Applications and Future Prospects. *Biomolecules*. 2021; 11(6): 886. <https://doi.org/10.3390/biom11060886> PMID: 34203733
35. Arenas-Salinas M, Vargas-Pérez JI, Morales W, Pinto C, Muñoz-Díaz P, Cornejo FA, et al. Flavoprotein-Mediated Tellurite Reduction: Structural Basis and Applications to the Synthesis of Tellurium-Containing Nanostructures. *Front Microbiol*. 2016; 7: 1160. <https://doi.org/10.3389/fmicb.2016.01160> PMID: 27507969
36. Castro ME, Molina R, Díaz W, Pichuantes SE, Vásquez CC. The dihydrolipoamide dehydrogenase of *Aeromonas caviae* ST exhibits NADH dependent tellurite reductase activity. *Biochem Biophys Res Commun*. 2008; 375(1): 91–94.
37. Choi Y, Park TJ, Lee DC, Lee SY. Recombinant *Escherichia coli* as a biofactory for various single- and multi-element nanomaterials. *Proc Natl Acad Sci U S A*. 2018; 115(23): 5944–5949.
38. Mandal D, Bolander ME, Mukhopadhyay D, Sarkar G, Mukherjee P. The use of microorganisms for the formation of metal nanoparticles and their application. *Appl Microbiol Biotechnol*. 2006; 69: 485–492. <https://doi.org/10.1007/s00253-005-0179-3> PMID: 16317546
39. Emam HE, Ahmed HB. Comparative study between homo-metallic & hetero-metallic nanostructures based agar in catalytic degradation of dyes. *Int. J. Biol. Macromol*. 2019; 138: 450–461.
40. Emam HE, Saad NM, Abdallah AEM, Ahmed HB. Acacia gum versus pectin in fabrication of catalytically active palladium nanoparticles for dye discoloration. *Int J Biol Macromol*. 2020; 156: 829–840. <https://doi.org/10.1016/j.ijbiomac.2020.04.018> PMID: 32289427
41. Ahmed HB, Emam HE. Overview for multimetallic nanostructures with biomedical, environmental and industrial applications. *J Mol Li*. 2021; 321: 114669.
42. Hassabo AA, Ibrahim EI, Ali BA, Emam HE. Anticancer effects of biosynthesized Cu₂O nanoparticles using marine yeast. *Biocatal Agric Biotechnol*; 2022; 39: 102261.
43. Singh RS, Rangari VK, Sanagapalli S, Jayaramana V, Mahendras S, Singha VP. Nano-Structured CdTe, CdS and TiO₂ for Thin Film Solar Cell Applications. *Sol Energy Mater. Sol. Cells* 2004; 82: 315.
44. Schneider T, Baldauf A, Ba LA, Jamier V, Khairan K, Sarakbi MB, et al. Selective antimicrobial activity associated with sulfur nanoparticles. *J Biomed Nanotechnol*. 2011; 7(3): 395–405. <https://doi.org/10.1166/jbn.2011.1293> PMID: 21830480
45. Demir R, Okur S, Seeker M. Electrical characterization of CdS nanocrystals for humidity sensing applications. *Ind Eng Chem Res*. 2012; 51: 3309–3313.

46. Rajeshkumar S, Ponnaiyandurai M, Malarkodi C, Malini M, Annadurai G. Microbe-mediated synthesis of antimicrobial semiconductor nanoparticles by marine bacteria. *J Nanostruct Chem*. 2014; 4: 96.
47. Raj R, Das S. Development and application of anticancer fluorescent CdS nanoparticles enriched *Lactobacillus* bacteria as therapeutic microbots for human breast carcinoma. *Appl Microbiol Biotechnol*. 2017; 101: 5439–5451. <https://doi.org/10.1007/s00253-017-8298-1> PMID: 28455616
48. Tripathi RM, Pragadeeshwara Rao R, Tsuzuki T. Green synthesis of sulfur nanoparticles and evaluation of their catalytic detoxification of hexavalent chromium in water. *RSC Adv*. 2018; 8: 36345–36352. <https://doi.org/10.1039/c8ra07845a> PMID: 35558482
49. Presentato A, Piacenza E, Darbandi A, Anikovskiy M, Cappelletti M, Zannoni D, et al. Assembly, growth and conductive properties of tellurium nanorods produced by *Rhodococcus aetherivorans* BCP1. *Sci Rep* 2018; 8: 3923.
50. Gahlawat G, & Choudhury AR. A review on the biosynthesis of metal and metal salt nanoparticles by microbes. *RSC advances*. 2019; 9(23): 12944–12967. <https://doi.org/10.1039/c8ra10483b> PMID: 35520790
51. Wang K, Zhang X, Kislyakov IM, Dong N, Zhang S, Wang G, et al. Bacterially synthesized tellurium nanostructures for broadband ultrafast nonlinear optical applications. *Nat. Commun*. 2019; 10: 3985. <https://doi.org/10.1038/s41467-019-11898-z> PMID: 31484932
52. Castro L, Li J, González F, Muñoz JA, Blásquez ML. Green synthesis of tellurium nanoparticles by tellurate and tellurite reduction using *Aeromonas hydrophila* under different aeration conditions. *Hydrometallurgy* 2020; 196: 105415.
53. Dabhane H, Ghotekar S, Tambade P, Pansambal S, Ananda Murthy HC, Oza R, et al. A review on environmentally benevolent synthesis of CdS nanoparticle and their applications. *Environ. Chem. Ecotoxicol*. 2021; 3: 209–219.
54. Shankar S, Jaiswal L, Rhim JW. New insight into sulfur nanoparticles: Synthesis and applications. *Crit Rev Environ Sci Technol*. 2021; 51(20): 2329–2356.
55. Zambonino MC, Quizhpe EM, Jaramillo FE, Rahman A, Santiago Vispo N, Jeffryes C, et al. Green Synthesis of Selenium and Tellurium Nanoparticles: Current Trends, Biological Properties and Biomedical Applications. *Int J Mol Sci*. 2021; 22(3): 989. <https://doi.org/10.3390/ijms22030989> PMID: 33498184
56. Dey PC, Ingti B, Bhattacharjee A, Choudhury MD, Das R, Nath SS. Enhancement of antibacterial activity of synthesized ligand-free CdS nanocrystals due to silver doping. *J Basic Microbiol*. 2021; 61(1): 27–36. <https://doi.org/10.1002/jobm.202000296> PMID: 33164242